Supporting information for

The effect of methyl group rotation on ^{1}H-^{1}H solid-state NMR spin-diffusion spectra

Ettore Bartalucci[a,b], Dominique Luder[b,c], Nicole Terefenko[b], Alexander A. Malär[d], Carsten Bolm[e], Matthias Ernst[c,*] and Thomas Wiegand[a,b,*]

[a] Max Planck Institute for Chemical Energy Conversion, Stiftstr. 34-36, 45470 Mülheim/Ruhr, Germany

[b] Institute of Technical and Macromolecular Chemistry, RWTH Aachen University, Worringerweg 2, 52074 Aachen, Germany

[c] Physical Chemistry, ETH Zürich, Vladimir-Prelog-Weg 2, 8093 Zürich, Switzerland

[d] Fraunhofer Headquarters, Hansastr. 27c, 80686 Munich, Germany

[e] Institute of Organic Chemistry, RWTH Aachen University, Landoltweg 1, 52074 Aachen, Germany

*: Corresponding authors. maer@ethz.ch and thomas.wiegand@cec.mpg.de

CH_{2b}-COOH [$(\omega^{(0)}_{CH2b} - \omega^{(0)}_{l}) + (\omega^{(0)}_{COOH} - \omega^{(0)}_{n})$]						
$\omega^{(0)}_{l}$ / $\omega^{(0)}_{n}$	CH_{2b}	CH_{2a}	H_a	NH_3	PO_3OH	COOH
CH_{2b}	12.8	12.6	11.6	8.5	4.1	0
CH_{2a}	12.6	12.4	11.4	8.3	3.9	-0.2
H_a	11.6	11.4	10.4	7.3	2.9	-1.2
NH_3	8.5	8.3	7.3	4.2	-0.2	-4.3
PO_3OH	4.1	3.9	2.9	-0.2	-4.6	-8.7
COOH	0	-0.2	-1.2	-4.3	-8.7	-12.8
CH_{2a}-COOH [$(\omega^{(0)}_{CH2a} - \omega^{(0)}_{l}) + (\omega^{(0)}_{COOH} - \omega^{(0)}_{n})$]						
$\omega^{(0)}_{l}$ / $\omega^{(0)}_{n}$	CH_{2b}	CH_{2a}	H_a	NH_3	PO_3OH	COOH
CH_{2b}	13	12.8	11.8	8.7	4.3	0.2
CH_{2a}	12.8	12.6	11.6	8.5	4.1	0
H_a	11.8	11.6	10.6	7.5	3.1	-1
NH_3	8.7	8.5	7.5	4.4	0	-4.1
PO_3OH	4.3	4.1	3.1	0	-4.4	-8.5
COOH	0.2	0	-1	-4.1	-8.5	-12.6
H_a-COOH [$(\omega^{(0)}_{Ha} - \omega^{(0)}_{l}) + (\omega^{(0)}_{COOH} - \omega^{(0)}_{n})$]						
$\omega^{(0)}_{l}$ / $\omega^{(0)}_{n}$	CH_{2b}	CH_{2a}	H_a	NH_3	PO_3OH	COOH
CH_{2b}	14	13.8	12.8	9.7	5.3	1.2
CH_{2a}	13.8	13.6	12.6	9.5	5.1	1
H_a	12.8	12.6	11.6	8.5	4.1	0
NH_3	9.7	9.5	8.5	5.4	1	-3.1
PO_3OH	5.3	5.1	4.1	1	-3.4	-7.5
COOH	1.2	1	0	-3.1	-7.5	-11.6
CH_{2b}-PO_3OH [$(\omega^{(0)}_{CH2b} - \omega^{(0)}_{l}) + (\omega^{(0)}_{PO3OH} - \omega^{(0)}_{n})$]						
$\omega^{(0)}_{l}$ / $\omega^{(0)}_{n}$	CH_{2b}	CH_{2a}	H_a	NH_3	PO_3OH	COOH
CH_{2b}	8.7	8.5	7.5	4.4	0	-4.1
CH_{2a}	8.5	8.3	7.3	4.2	-0.2	-4.3
H_a	7.5	7.3	6.3	3.2	-1.2	-5.3
NH_3	4.4	4.2	3.2	0.1	-4.3	-8.4
PO_3OH	0	-0.2	-1.2	-4.3	-8.7	-12.8
COOH	-4.1	-4.3	-5.3	-8.4	-12.8	-16.9
CH_{2a}- PO_3OH [$(\omega^{(0)}_{CH2a} - \omega^{(0)}_{l}) + (\omega^{(0)}_{PO3OH} - \omega^{(0)}_{n})$]						
$\omega^{(0)}_{l}$ / $\omega^{(0)}_{n}$	CH_{2b}	CH_{2a}	H_a	NH_3	PO_3OH	COOH
CH_{2b}	8.9	8.7	7.7	4.6	0.2	-3.9
CH_{2a}	8.7	8.5	7.5	4.4	0	-4.1
H_a	7.7	7.5	6.5	3.4	-1	-3.2
NH_3	4.6	4.4	3.4	0.3	-4.1	-8.2
PO_3OH	0.2	0	-1	-4.1	-8.5	-12.6
COOH	-3.9	-4.1	-5.1	-8.2	-12.6	-16.7

Table S1: Calculations for negative cross peaks of **1** originating from the coherent third-order SD condition involving four spins. The values are obtained from the resonance condition [$(\omega^{(0)}_{k} - \omega^{(0)}_{l}) + (\omega^{(0)}_{m} - \omega^{(0)}_{n}) \sim 0$] using the experimental chemical shifts of **1** (ω_{CH2a} = 4.2 ppm, ω_{CH2b} = 4.0 ppm, ω_{Ha} = 5.2 ppm, ω_{NH3} = 8.3 ppm. ω_{PO3OH} = 12.7 ppm, ω_{COOH} = 16.8 ppm). The values highlighted in red are those values close to the fulfilment of the resonance conditions.

CH_3-COOH $[(\omega^{(0)}_{CH3} - \omega^{(0)}_{l}) + (\omega^{(0)}_{COOH} - \omega^{(0)}_{n})]$			
$\omega^{(0)}_{l}$ / $\omega^{(0)}_{n}$	CH_3	OH	COOH
CH_3	10	5.3	0
OH	5.3	0.6	-4.7
COOH	0	-4.7	-10
CH_3-OH $[(\omega^{(0)}_{CH3} - \omega^{(0)}_{l}) + (\omega^{(0)}_{OH} - \omega^{(0)}_{n})]$			
$\omega^{(0)}_{l}$ / $\omega^{(0)}_{n}$	CH_3	OH	COOH
CH_3	4.7	0	-5.3
OH	0	-4.7	-10
COOH	-5.3	-10	-15.3
OH-COOH $[(\omega^{(0)}_{OH} - \omega^{(0)}_{l}) + (\omega^{(0)}_{COOH} - \omega^{(0)}_{n})]$			
$\omega^{(0)}_{l}$ / $\omega^{(0)}_{n}$	CH_3	OH	COOH
CH_3	14.7	10	4.7
OH	10	5.3	0
COOH	4.7	0	-4.7

Table S1 - continued: Calculations for negative cross peaks of **2** originating from the coherent third-order SD condition involving four spins. The values are obtained from the resonance condition $[(\omega^{(0)}_{k} - \omega^{(0)}_{l}) + (\omega^{(0)}_{m} - \omega^{(0)}_{n}) \sim 0]$ using the experimental chemical shifts of **2** (ω_{CH3} = 1.6 ppm, ω_{OH}= 6.3 ppm and ω_{COOH} = 11.6 ppm). The values highlighted in red are those values close to the fulfilment of the resonance conditions.

CH_3-H_{arom} (4/7) $[(\omega^{(0)}_{CH3} - \omega^{(0)}_{l}) + (\omega^{(0)}_{Harom} - \omega^{(0)}_{n})]$				
$\omega^{(0)}_{l}$ / $\omega^{(0)}_{n}$	CH_3	CH_2	H_{arom}(5/6)	H_{arom}(4/7)
CH_3	4.7	3.2	0.9	0
CH_2	3.2	1.7	-0.6	-1.5
H_{arom}(5/6)	0.9	-0.6	-2.9	-3.8
H_{arom}(4/7)	0	-1.5	-3.8	-4.7
CH_3-H_{arom} (5/6) $[(\omega^{(0)}_{CH3} - \omega^{(0)}_{l}) + (\omega^{(0)}_{Harom} - \omega^{(0)}_{n})]$				
$\omega^{(0)}_{l}$ / $\omega^{(0)}_{n}$	CH_3	CH_2	H_{arom}(5/6)	H_{arom}(4/7)
CH_3	3.8	2.3	0	-0.9
CH_2	2.3	0.8	-1.5	-2.4
H_{arom}(5/6)	0	-1.5	-3.8	-4.7
H_{arom}(4/7)	-0.9	-2.4	-4.7	-5.6

Table S1 - continued: Calculations for negative cross peaks of **3** originating from the coherent third-order SD condition involving four spins. The values are obtained from the resonance condition $[(\omega^{(0)}_{k} - \omega^{(0)}_{l}) + (\omega^{(0)}_{m} - \omega^{(0)}_{n}) \sim 0]$ using the experimental chemical shifts of **3** (ω_{CH3} = 2.7 ppm, ω_{CH2} = 4.2 ppm. $\omega_{Harom5/6}$ = 6.5 ppm and $\omega_{Harom4/7}$ = 7.4 ppm). The values highlighted in red are those values close to the fulfilment of the resonance conditions.

CH_3^b-H_{arom}^a $[(\omega^{(0)}_{CH3b} - \omega^{(0)}_l) + (\omega^{(0)}_{Haroma} - \omega^{(0)}_n)]$					
$\omega^{(0)}_l$ / $\omega^{(0)}_n$	CH_{3b+a}	CH_{3a}	CH	H_{arom}^a	H_{arom}^b
CH_3^{b+a}	5.6	4.6	3.8	0	0.7
CH_3^a	4.6	3.6	2.8	-1	-0.3
CH	3.8	2.8	2	-1.8	-1.1
H_{arom}^a	0	-1	-1.8	-5.6	-4.9
H_{arom}^b	0.7	-1.7	-2.5	-4.7	-4

Table S1 - continued: Calculations for negative cross peaks of **4** originating from the coherent third-order SD condition involving four spins. The values are obtained from the resonance condition $[(\omega^{(0)}_k - \omega^{(0)}_l) + (\omega^{(0)}_m - \omega^{(0)}_n) \sim 0]$ using the experimental chemical shifts of **4** (ω_{CH3b+a} = 1 ppm, ω_{CH3a} = 2 ppm, ω_{CH} = 2.8 ppm, ω_{Haroma} = 6.6 ppm. ω_{Haromb} = 5.9 ppm). The values highlighted in red are those values close to the fulfilment of the resonance conditions. [a]: H5/H9 and [b]: H6/H8.

Compound / δ(^{1}H) ppm	Sulfoximine **3**	$RuCl_2$-cymene **4**	Bora[4]pyramidane **5**	Durene **6**
H_{arom}	H_{arom} (4/7) = 7.4 H_{arom} (5/6) = 6.5	H_{arom}^a = 6.6 H_{arom}^b = 5.9	/	6.6
CH	/	2.8	5.6	/
CH_2	4.2	/	/	/
CH_3	2.7	CH_3^{a+b} = 1.1/0.9 $CH_3^{a'}$ = 2.0	-0.1	1.3

Table S2: Proton chemical shift values tabulated for the assigned resonances in the ^{1}H MAS spectra in Figure 3.

Compound / δ(^{1}H) ppm	**CH_3**	**OH**	**COOH**	**Δδ(CH_3···OH)/ ppm**	**Δδ(OH···COOH)/ ppm**
Rac-TLa **6**	1.6	6.3	11.6	4.7	5.3

Table S2 Continued: Proton chemical shift values tabulated for the α-TLa **2** racemate compound resonances. Reported is also the chemical shift differences between methyl and hydroxyl protons and the hydroxyl and carboxylic protons.

Discussion of negative cross peaks observed for compounds 2 and 3.

In case of α-TLA, at 50 ms mixing time negative cross peaks are observed between the methyl group protons at 1.6 ppm and the carboxylic protons at 11.6 ppm. And indeed, the chemical-shift difference of the hydroxyl proton and the methyl-group protons roughly matches the differences in chemical shifts between the carboxylic proton and the hydroxyl proton (with chemical-shift differences of $\omega_{OH} - \omega_{CH_3} = 4.7\ ppm$ and $\omega_{COOH} - \omega_{OH} = 5.3\ ppm$, respectively). At shorter mixing times (i.e. Figure 3a with τ_{mix} = 1 ms) for α-TLA, further negative cross peaks between the CH_3 and OH protons and the OH and COOH protons are observed, which become positive upon increasing the mixing time (Figure 3b and Figure S3). This observation can be explained since the second-order SD term becomes again a progressively dominant factor at longer mixing times, thus resulting in positive off diagonal peaks, which is in agreement with the reported example of histidine·HCl·H_2O.[1] The different cross peak build-up rates for the negative peaks of α-TLA can be rationalized therefore by an interplay between chemical-shift separation and SD mixing time.

A similar case, albeit slightly more complex, is represented by sulfoximine **3**. Also for this system the coherent third-order condition mentioned above can be fulfilled (Table S1) for the collection of proton spins: CH_3 = 2.7 ppm, CH_2 = 4.2 ppm, H_{arom}(5/6) = 6.5 ppm and H_{arom}(4/7) = 7.4 ppm, leading to negative cross peaks in the 2D spectrum (Figure 4a). However, a full compensation of chemical shifts according to the above-mentioned equation is not observed (difference of 0.6 ppm in the chemical-shift differences). The last example in this line, namely the $RuCl_2$-cymene complex **4** reveals a negative cross peak between the methyl group CH_3^b (1 ppm) and the aromatic protons H5/H9 (6.6 ppm), see Figure 4b. Again, by taking into account the CH_3^a protons (2 ppm) and aromatic protons H6/H8 (5.9 ppm) as further spins in the quadruple of spins, the resonance condition is approximately fulfilled (difference of 0.7 ppm in the chemical-shift differences.

Supplementary Figures

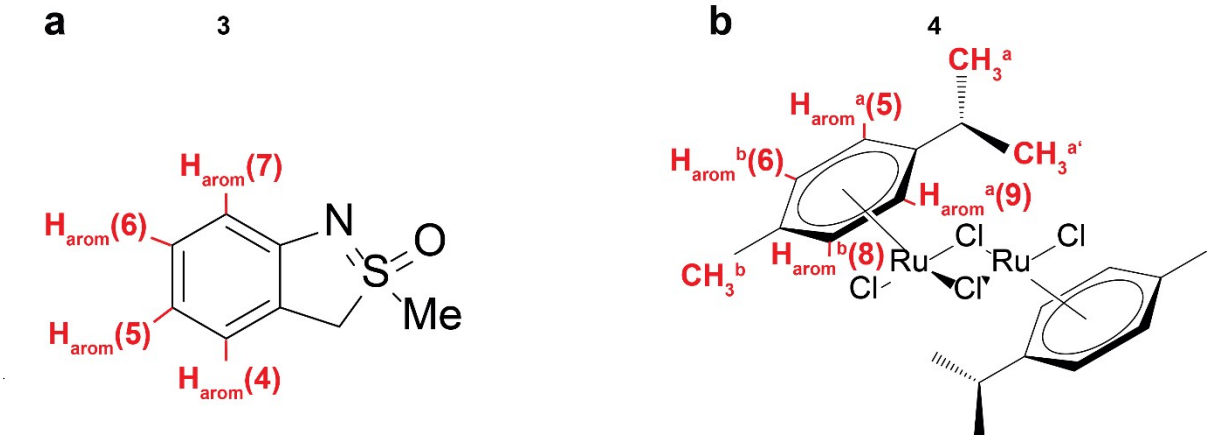

Figure S1: Atom nomenclature used in the ^{1}H MAS spectra of compounds **3** and **4.**

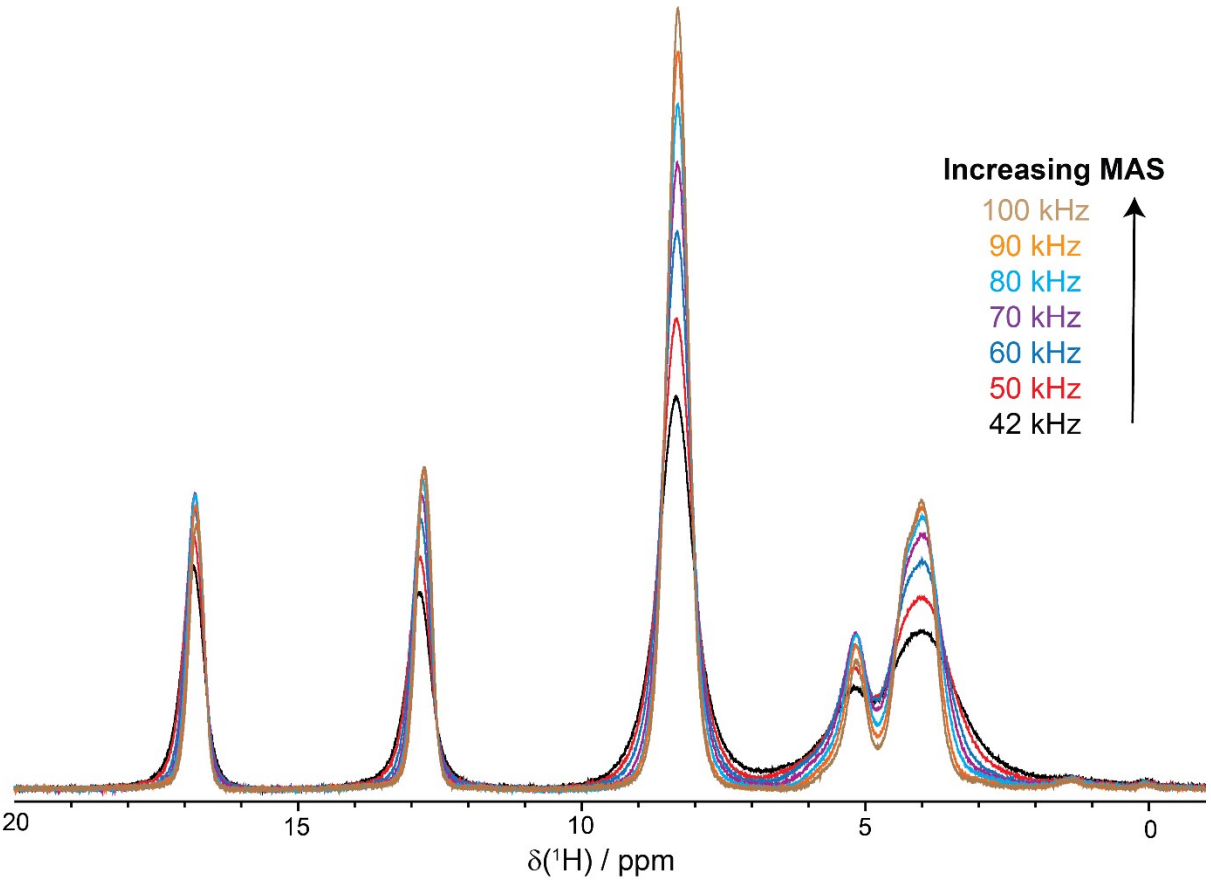

Figure S2: *^{1}H line widths dependence upon increasing the MAS frequency*.1D ^{1}H MAS spectra recorded with different MAS frequencies of *O*-phospho-L-serine **1** measured at 16.4 T static magnetic-field strength.

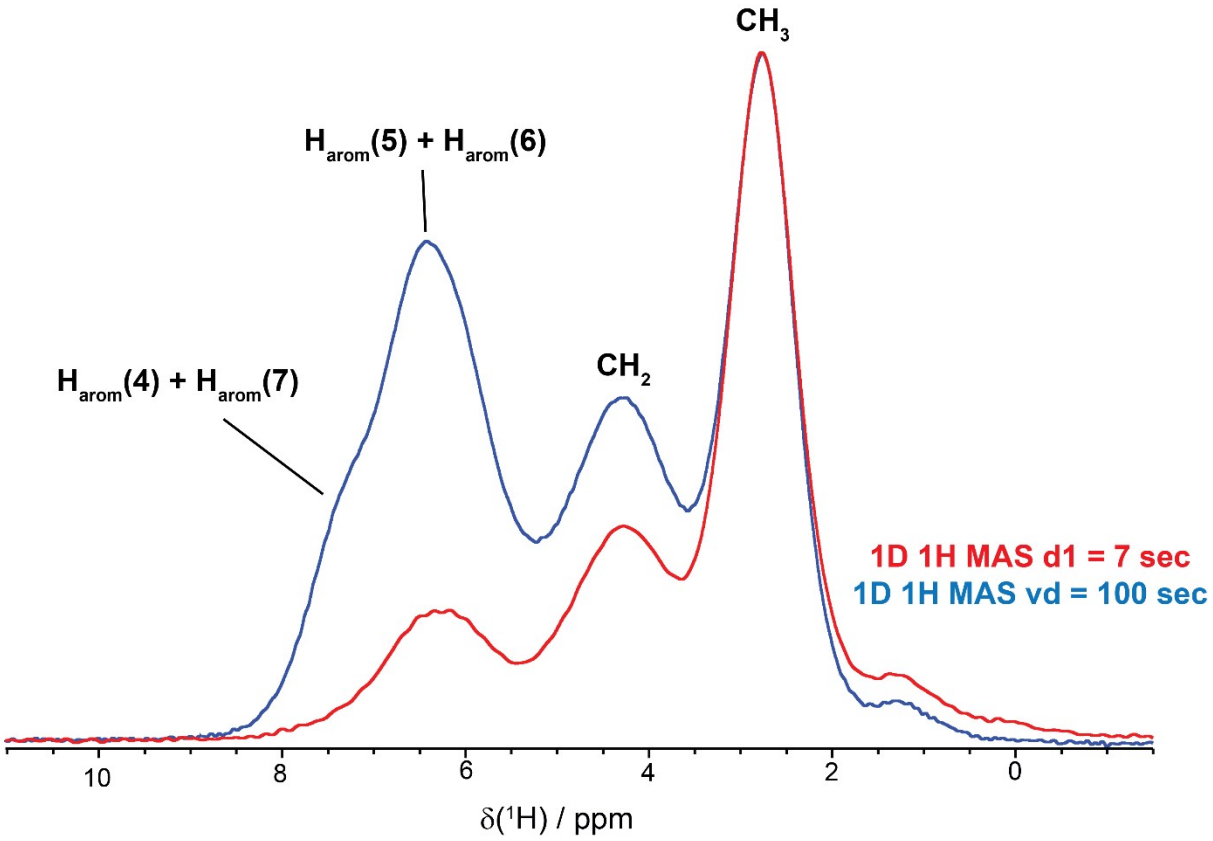

Figure S3: 1D ^{1}H MAS spectra of sulfoximine **3** recorded with a d1 = 7 s (red) and a 1D slice of the ^{1}H saturation recovery experiment recorded with a delay of 100 s (blue). We clearly see the shoulder for the H4/H7 aromatic protons showing up.

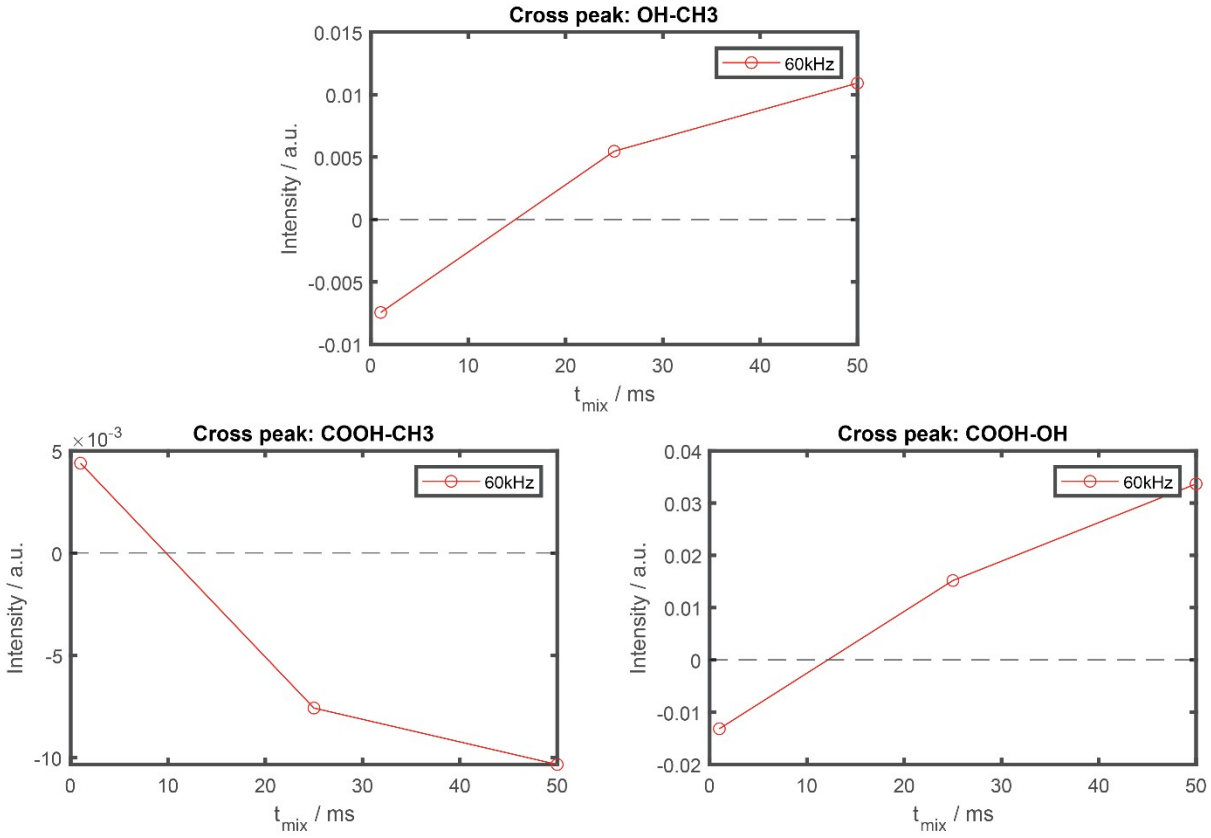

Figure S4: Mixing-time dependence of the integrated intensities for negative cross peaks (normalized with respect to the methyl-group diagonal peak at t_{mix}=1 ms) of α-TLA. The 2D SD spectra from which the intensities have been extracted were recorded at 60 kHz MAS frequency and 16.4 T static magnetic-field strength.

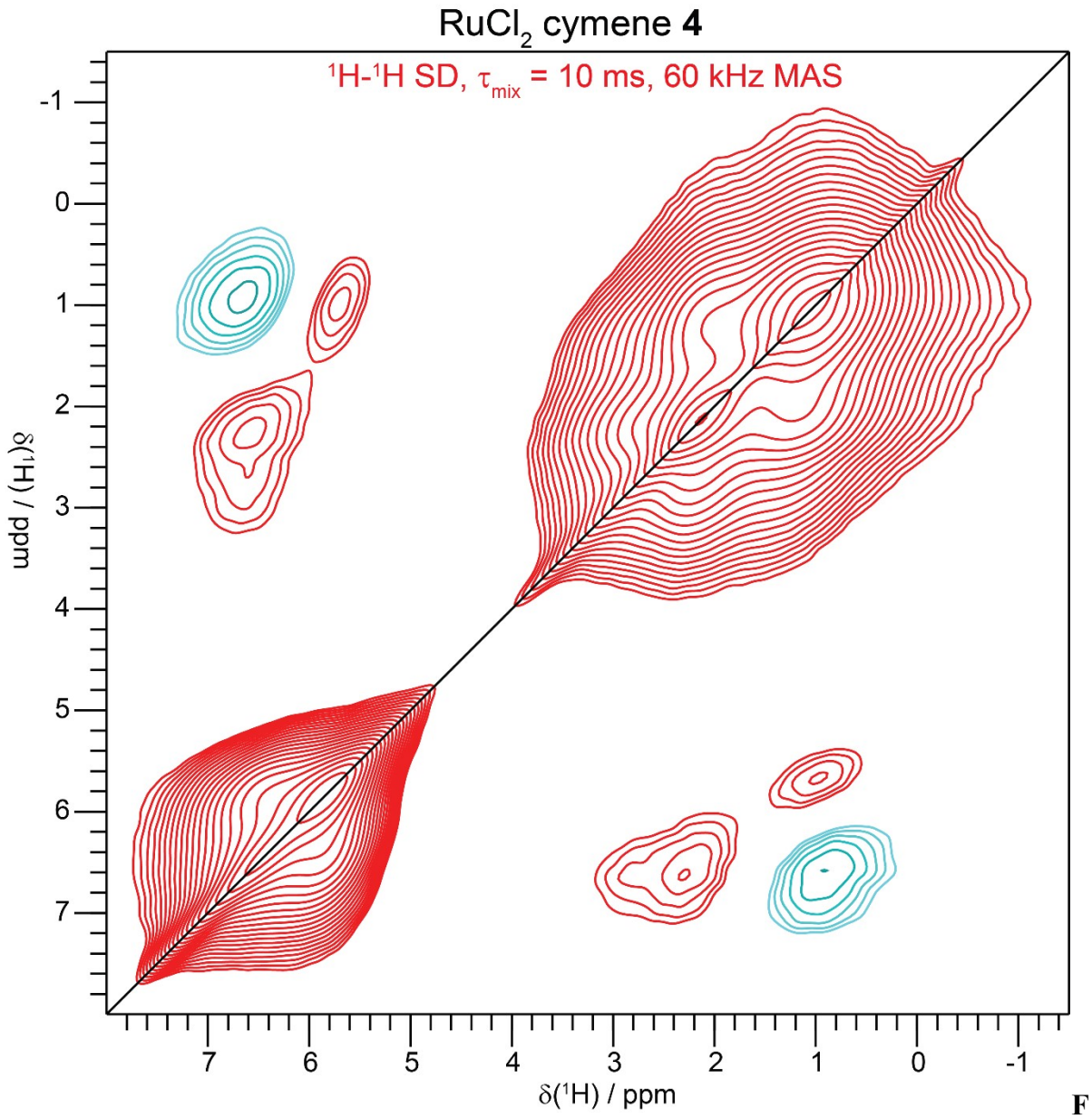

igure S5: 2D ^{1}H-^{1}H SD spectrum of **4** recorded with 10 ms mixing time at 60 kHz MAS frequency at 16.4 T static magnetic-field strength.

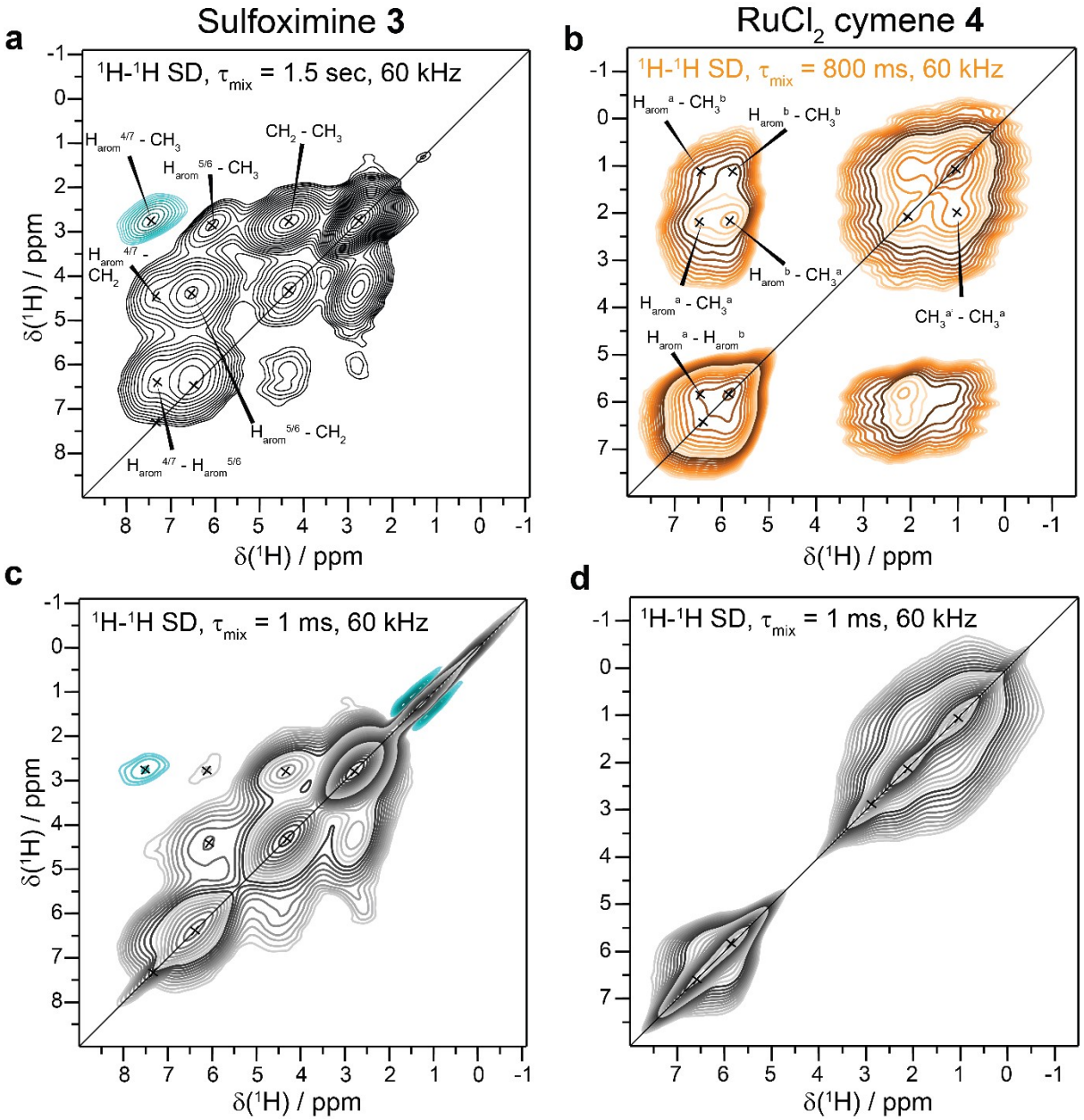

Figure S6: 2D ^{1}H-^{1}H SD spectra of **3** (**a**,**c**) and **4** (**b**,**d**) recorded with **a** 1.5 s, **b** 800 ms, **c** 1 ms and **d** 1 ms mixing times. All spectra have been recorded at 60 kHz MAS frequency on a 16.4 T static magnetic field strength.

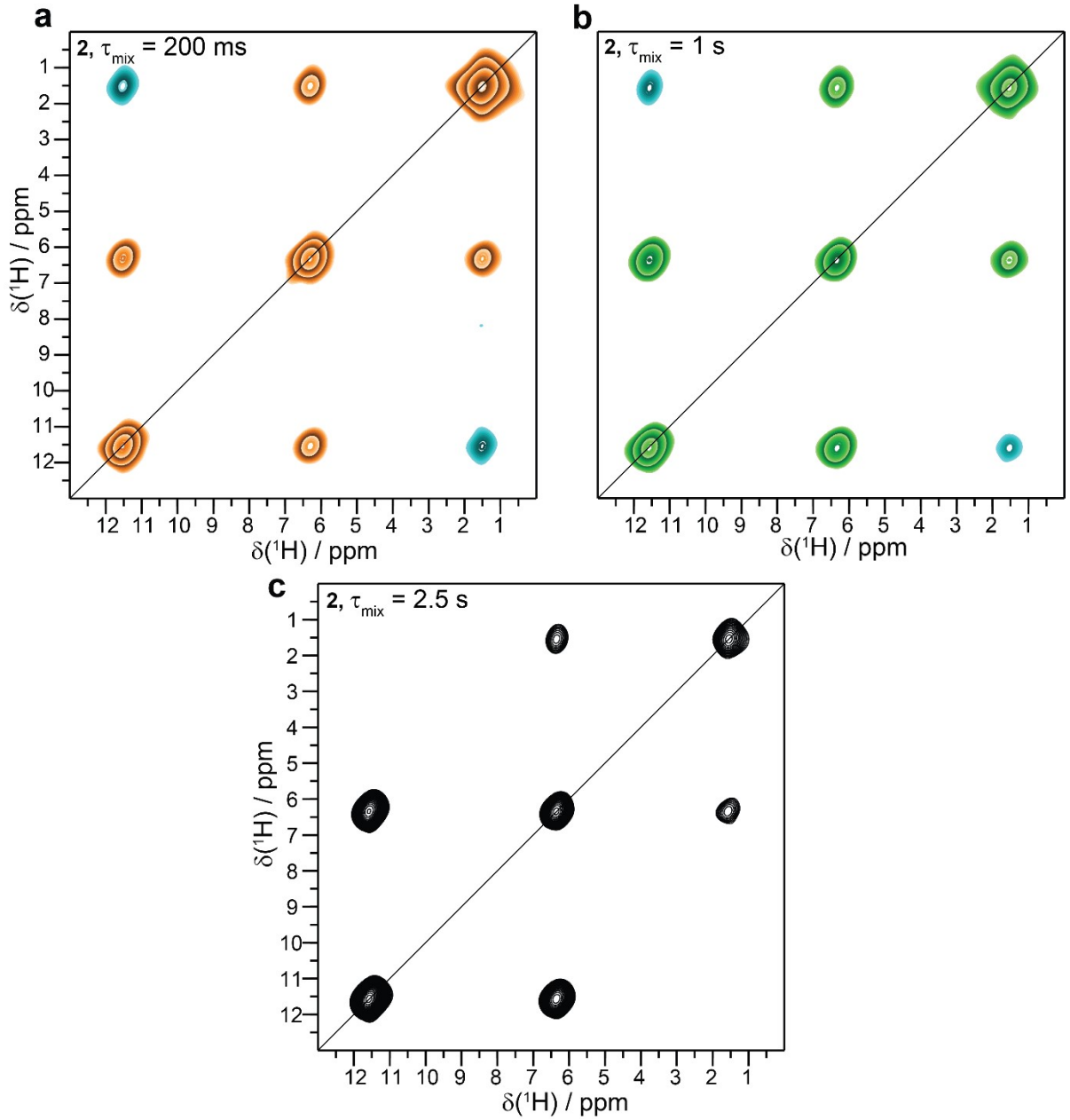

Figure S7: 2D ^{1}H-^{1}H SD spectra of **2** recorded with **a** 200 ms, **b** 1 s and **c** 2.5 s mixing times. All spectra have been recorded at 60 kHz MAS frequency at 16.4 T static magnetic-field strength.

Details of the analytic simulations

We assume a H_3-H spin system where the three equivalent protons are part of a CH_3 group that undergoes stochastic jumps around the symmetry axis. All dipolar couplings can be characterized in a coordinate system where the z axis is aligned with the symmetry axis of the CH_3 group and the x axis can be chosen arbitrarily. The correlation function is then given by

$$C_{2,2,m,m}^{(\mu,\mu')}(\tau) = A_{2,m}^{(\mu)}(t)A_{2,m}^{(\mu')*}(t-\tau).$$

To calculate the correlation function, we apply three Euler transformations from the principal-axes system to the methyl-fixed frame ($D_{0,m}^{2}(0,\theta^{(\mu)}(t),\phi^{(\mu)}(t))$), then to the rotor fixed frame ($D_{m',m}^{2}(\alpha,\beta,\gamma)$) and finally to the laboratory frame ($D_{m,m'}^{2}(-\omega_r t,-\theta_m,0)$). Therefore, the spherical tensors in the laboratory frame can be written as:

$$A_{2,m}^{(\mu)}(t) = \sum_{m'=-2}^{2}\sum_{m''=-2}^{2} D_{m,m'}^{2}(-\omega_r t,-\theta_m,0)D_{m',m''}^{2}(\alpha,\beta,\gamma)D_{0,m''}^{2}(0,\theta^{(\mu)}(t),\phi^{(\mu)}(t))\rho_{2,0}^{(\mu)}.$$

To calculate the correlation function, we introduce discrete values for the angles $\theta^{(\mu)}(t)$ and $\phi^{(\mu)}(t)$, $\theta_i^{(\mu)}$ and $\phi_i^{(\mu)}$ and a correlation function defined by

$$C_{i,j}(t) = \frac{1}{3}\left(\frac{1}{3} + \left(\delta_{i,j} - \frac{1}{3}\right)e^{-\frac{t}{\tau_j}}\right)$$

where $\tau_j = \frac{1}{3k_j}$ is the correlation time of the jump process. The total correlation function is then given by

$$C_{2,2,m,m}^{(\mu,\mu')}(t) = \rho_{2,0}^{(\mu)}\rho_{2,0}^{(\mu')}\sum_{i,j=1}^{3}\sum_{m',k'=-2}^{2}\sum_{m'',k''=-2}^{2} D_{m,m'}^{2}(-\omega_r t,-\theta_m,0)D_{m'',m}^{2}$$
$$D_{0,m''}^{2}(0,\theta_i^{(\mu)},\phi_i^{(\mu)})\left(D_{k,k'}^{2}(-\omega_r t,-\theta_m,0)D_{k'',k}^{2}(\alpha,\beta,\gamma)D_{0,k}^{2}(\right.$$

The orientation-dependent and MAS-dependent spectral density function can now be calculated as:

$$J_{m}^{(\mu,\mu')}(\omega) = \rho_{2,0}^{(\mu)}\rho_{2,0}^{(\mu')}\sum_{i,j=1}^{3}\sum_{m',k'=-2}^{2}\sum_{m'',k''=-2}^{2} D_{m,m'}^{2}(-\omega_r t,-\theta_m,0)D_{m'',m}^{2}$$
$$D_{0,m''}^{2}(0,\theta_i^{(\mu)},\phi_i^{(\mu)})\left(D_{k,k'}^{2}(-\omega_r t,-\theta_m,0)D_{k'',k}^{2}(\alpha,\beta,\gamma)D_{0,k}^{2}(0,\theta_j^{(\mu')},\right.$$

Analytical integration over the Euler angles (α,β,γ) describing the crystallite orientation (powder average) and the rotor cycle leads to the spectral-density functions that can be inserted into Eqs. (2)-(4) of the main manuscript.

The coordinates of the four protons considered in the analytical calculations are given by:

C1 (+0.0000, +0.0000, +-0.3264) Å
H1A (-0.8677, -0.3185, +0.0000) Å
H1B (+0.1578, +0.9107, +0.0000) Å
H1C (+0.7100, -0.5913, +0.0000) Å
H6 (+0.9006, +2.2099, +2.2954) Å

Details of the numerical simulations

All numerical simulations were carried out in the spin-simulation environment GAMMA.[2] The simulations were carried out in the laboratory frame including the Zeeman Hamiltonian, the isotropic chemical shifts and the untruncated dipolar couplings between all spins. The magnitude and orientation of the dipolar couplings were calculated based on the geometry of the spin system. For the simulations of the four proton spins representing the relevant part of sulfoximine **3**, the coordinates used for the analytical calculations were used. The isotropic chemical-shift difference between the methyl and the aromatic protons was set to 10 kHz to minimize spin-diffusion based polarization transfer. For the six-spin simulations, which also included the methylene group, the coordinates of the atoms are given by:

C1 (3.446, 1.682, 9.719) Å
H1A (2.692, 1.925, 10.296) Å
H1B (4.237, 2.199, 9.982) Å
H1C (3.635, 0.725, 9.814) Å
H2A (2.339, 4.233, 7.573) Å
H2B (3.688, 4.265, 8.464) Å
H6 (4.015, 5.668, 5.780) Å

They were selected such that the distance between the methyl-group protons and the methylene protons (2.6 Å) and the methylene and the aromatic proton (2.8 Å) was minimized to facilitate third-order spin diffusion. The chemical shifts were set to 1630 Hz (methyl), 3430 Hz (methylene) and 5230 Hz (aromatic) which matches the third-order spin-diffusion condition perfectly.

The time-dependence due to MAS was simulated using time slicing of the time-dependent Hamiltonian. In addition, an exchange process simulating the stochastic exchange of the three methyl-group protons was added in the Liouville space. Powder averaging was done using the ZCW grid with either 100 (six-spin system) or 300 powder orientations (four-spin system). Computation times were about one hour for the four-spin system and 800 hours for the six-spin system.

To demonstrate how the cross relaxation depends on the minimum distance between the methyl protons and the fourth proton, model spin systems based on an ideal methyl group were calculated. The fourth spin was located on the rotation axis of the methyl group and moved away from the plane of the three methyl protons. In a second set of simulations, the fourth proton was located in the plane of the three methyl protons and moved away from the nearest proton in the plane. Figure S8 shows the cross-relaxed magnetization as a function of the mixing time for different minimum distances between the fourth proton and the nearest methyl-

group proton. One can clearly see that very short distances are required to obtain significant polarization transfer.

The coordinates of the four protons for the axial model are given by (H1A, H1B, H1C are the coordinates of the methyl protons, H4X are the coordinates of the fourth proton used in the five different simulations):

C1 (0.0000, 0.0000, 0.0000) Å
H1A (1.0698, 0.0000, 0.3789) Å
H1B (0.5345, 0.9265, 0.3789) Å
H1C (0.5345, -0.9265, 0.3789) Å
H4A (0.0000, 0.0000, 0.3789) Å
H4B (0.0000, 0.0000, 1.4303) Å
H4C (0.0000, 0.0000, 2.0687) Å
H4D (0.0000, 0.0000, 2.6384) Å
H4E (0.0000, 0.0000, 3.1817) Å

The coordinates of the four protons for the planar model are given by (H1A, H1B, H1C are the coordinates of the methyl protons, H4X are the coordinates of the fourth proton used in the five different simulations):

C1 (0.0000, 0.0000, 0.0000) Å
H1A (1.0698, 0.0000, 0.3789) Å
H1B (0.5345, 0.9265, 0.3789) Å
H1C (0.5345, -0.9265, 0.3789) Å
H4A (2.0698, 0.0000, 0.3789) Å
H4B (2.5698, 0.0000, 0.3789) Å
H4C (3.0698, 0.0000, 0.3789) Å
H4D (3.5698, 0.0000, 0.3789) Å
H4E (4.0698, 0.0000, 0.3789) Å

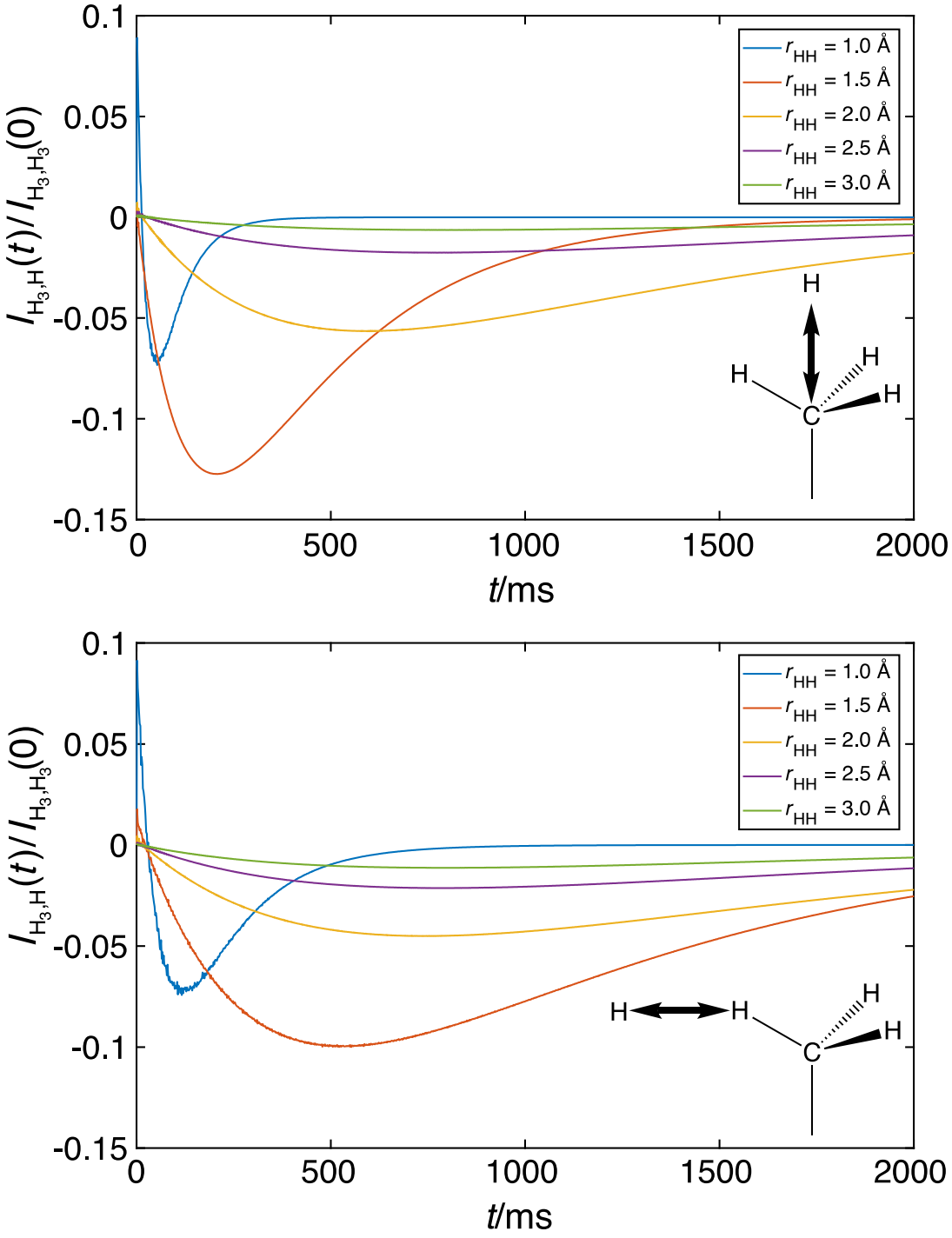

Figure S8: Numerical simulations of the cross relaxation between the methyl-group protons and a fourth proton either located on the rotation axis (a) or in the plane of the three methyl protons (b) as a function of the minimum distance. Significant cross relaxation for the chosen jump correlation time of $\tau_j \approx 8.7 \cdot 10^{-11}$ s was only obtained for very short distances.

Table S3: Overview about experimental parameters of the solid-state NMR measurements.

1D ^{1}H Hahn-echo	*O*-phospho-L-serine **1**	racemic α-TLA **2**	sulfoximine **3**	$RuCl_2$-cymene **4**	Bora[4]pyramidane **5**	durene **6**
ν_r / kHz	60	60	60	60	60	60
B_0 / T	16.4	16.4	16.4	16.4	16.4	16.4
$\nu_1(^1H)$ / kHz	100	100	100	100	100	100
^{1}H carrier / ppm	9.2	-6.6	25.2	21.6	3.1	24.8
t_1 increments	16384	16384	16384	16384	16384	16384
Sweep width (t_1) / ppm	142.8	142.8	142.8	142.8	142.8	142.8
Acquisition time (t_1) / ms	81.9	81.9	81.9	81.9	81.9	81.9
Interscan delay / s	2.7	6.5	7	7	10	7
Number of scans	16	16	4	16	16	16
Measurement time / sec	50	450	42	120	180	120
Probe target temperature / K	285	285	285	285	280	285

Continue of **Table S3**

1D ^{1}H Hahn-echo	*O*-phospho-L-serine **1**	*O*-phospho-L-serine **1**	*O*-phospho-L-serine **1**	*O*-phospho-L-serine **1**	*O*-phospho-L-serine **1**	*O*-phospho-L-serine **1**	*O*-phospho-L-serine **1**
ν_r / kHz	42	50	60	70	80	90	100
B_0 / T	16.4	16.4	16.4	16.4	16.4	16.4	16.4
$\nu_1(^1H)$ / kHz	150	150	150	150	150	150	150
^{1}H carrier / ppm	6.8	6.8	6.8	6.8	6.8	6.8	6.8
t_1 increments	16384	16384	16384	16384	16384	16384	16384
Sweep width (t_1) / ppm	142.8	142.8	142.8	142.8	142.8	142.8	142.8
Acquisition time (t_1) / ms	81.9	81.9	81.9	81.9	81.9	81.9	81.9
Interscan	1.5	1.5	1.5	1.5	1.5	1.5	1.5

delay / s							
Number of scans	16	16	4	16	16	16	16
Measurement time / sec	30	30	30	30	30	30	30
Probe target temperature / K	273	271	271	271	270	270	270

Continue of **Table S3**

2D ^{1}H-^{1}H Spin-Diffusion *O*-phospho-L-serine **1**	**50 ms**	**50 ms**	**2D ^{1}H-^{1}H RDFR** *O*-phospho-L-serine **1**	**320 µs**
ν_r/ kHz	60	100	ν_r/ kHz	100
B_0/ T	16.4	16.4	B_0/ T	16.4
Transfer	Spin Diffusion	Spin Diffusion	**Transfer**	Radiofrequency driven recoupling
ν_1(^{1}H) / kHz	100	150	ν_1(^{1}H) / kHz	150
SD Mixing Time / ms	50	50	RFDR Mixing Time / ms	0.32
^{1}H carrier/ ppm	9.2	6.8	^{1}H carrier/ ppm	6.8
t_1 increments	512	512	t_1 increments	400
Sweep width (t_1) / ppm	42.8	42.8	Sweep width (t_1) / ppm	42.8
Acquisition time (t_1)/ ms	8.5	8.5	Acquisition time (t_1)/ ms	6.6
t_2 increments	16384	16384	t_2 increments	16384
Sweep width (t_2)/ ppm	142.8	142.8	Sweep width (t_2)/ ppm	142.8
Acquisition time (t_2)/ ms	81.9	81.9	Acquisition time (t_2)/ ms	81.9
Interscan delay/ s	2.7	3	Interscan delay/ s	3
Number of scans	16	16	Number of scans	16
Measurement time/ min	388	428	Measurement time/ min	329
Probe target temperature / K	285	270	Probe target temperature /	270

			K	

Continue of **Table S3**

2D ^{1}H-^{1}H Spin-Diffusion racemic α-TLA **2**	**1 ms**	**50 ms**	**200 ms**	**1 s**	**2.5 s**
ν_r/ kHz	60	60	60	60	60
B_0/ T	16.4	16.4	16.4	16.4	16.4
Transfer	Spin Diffusion	Spin Diffusion	Spin Diffusion	Spin Diffusion	Spin Diffusion
ν_1(^{1}H) / kHz	100	100	100	100	100
SD Mixing Time / ms	1	50	200	1000	2500
^{1}H carrier/ ppm	-6.6	-6.6	1.7	1.7	1.7
t_1 increments	240	240	304	304	320
Sweep width (t_1) / ppm	42.8	42.8	42.8	42.8	42.8
Acquisition time (t_1)/ ms	4.0	4.0	5.0	5.0	5.0
t_2 increments	16384	16384	16384	16384	16384
Sweep width (t_2)/ ppm	142.8	142.8	142.8	142.8	142.8
Acquisition time (t_2)/ ms	81.9	81.9	81.9	81.9	81.9
Interscan delay/ s	6.5	6.5	6.5	6.5	6.5
Number of scans	16	16	16	16	16
Measurement time/ min	422	425	550	615	775
Probe target temperature / K	285	285	285	285	285

Continue of **Table S3**

2D ^{1}H-^{1}H Spin-Diffusion sulfoximine **3**	**1 ms**	**5 ms**	**20 ms**	**50 ms**	**100 ms**	**200 ms**
ν_r/ kHz	60	60	60	60	60	60
B_0/ T	16.4	16.4	16.4	16.4	16.4	16.4
Transfer	Spin Diffusion	Spin Diffusion	Spin Diffusion	Spin Diffusion	Spin Diffusion	Spin Diffusion
ν_1(^{1}H) / kHz	100	100	100	100	100	100
SD Mixing Time / ms	1	5	20	50	100	200
^{1}H carrier/ ppm	25.3	25.3	25.3	25.3	25.3	25.3

t_1 increments	500	500	500	500	500	500
Sweep width (t_1) / ppm	42.8	42.8	42.8	42.8	42.8	42.8
Acquisition time (t_1)/ ms	8.3	8.3	8.3	8.3	8.3	8.3
t_2 increments	16384	16384	16384	16384	16384	16384
Sweep width (t_2)/ ppm	142.8	142.8	142.8	142.8	142.8	142.8
Acquisition time (t_2)/ ms	81.9	81.9	81.9	81.9	81.9	81.9
Interscan delay/ s	7	7	7	7	7	7
Number of scans	16	16	16	16	16	16
Measurement time/ min	946	947	949	953	959	973
Probe target temperature / K	285	285	285	285	285	285

Continue of **Table S3**

2D ^{1}H-^{1}H Spin-Diffusion $RuCl_2$-cymene **4**	**1 ms**	**5 ms**	**10 ms**	**50 ms**	**800 ms**
ν_r/ kHz	60	60	60	60	60
B_0/ T	16.4	16.4	16.4	16.4	16.4
Transfer	Spin Diffusion	Spin Diffusion	Spin Diffusion	Spin Diffusion	Spin Diffusion
$\nu_1(^1H)$ / kHz	100	100	100	100	100
SD Mixing Time / ms	1	5	10	50	800
^{1}H carrier/ ppm	21.6	25.3	25.3	25.3	25.3
t_1 increments	500	500	500	500	500
Sweep width (t_1) / ppm	42.8	42.8	42.8	42.8	42.8
Acquisition time (t_1)/ ms	8.3	8.3	8.3	8.3	8.3
t_2 increments	16384	16384	16384	16384	16384
Sweep width (t_2)/ ppm	142.8	142.8	142.8	142.8	142.8
Acquisition time (t_2)/ ms	81.9	81.9	81.9	81.9	81.9
Interscan delay/ s	7	7	7	7	7
Number of scans	16	16	16	16	16
Measurement time/ min	946	947	947	953	1053
Probe target	285	285	285	285	285

temperature / K					

Continue of **Table S3**

2D ^{1}H-^{1}H Spin-Diffusion bora[4]pyramidane **5**	**50 ms**	**2D ^{1}H-^{1}H Spin-Diffusion** durene **6**	**50 ms**
ν_r/ kHz	60	ν_r/ kHz	60
B_0/ T	16.4	B_0/ T	16.4
Transfer	Spin Diffusion	**Transfer**	Spin Diffusion
ν_1(^{1}H) / kHz	100	ν_1(^{1}H) / kHz	100
SD Mixing Time / ms	50	SD Mixing Time / ms	50
^{1}H carrier/ ppm	5.1	^{1}H carrier/ ppm	24.8
t_1 increments	512	t_1 increments	436
Sweep width (t_1) / ppm	20	Sweep width (t_1) / ppm	42.8
Acquisition time (t_1)/ ms	18.3	Acquisition time (t_1)/ ms	7.2
t_2 increments	14336	t_2 increments	16384
Sweep width (t_2)/ ppm	140.9	Sweep width (t_2)/ ppm	142.8
Acquisition time (t_2)/ ms	72.6	Acquisition time (t_2)/ ms	81.9
Interscan delay/ s	7	Interscan delay/ s	7
Number of scans	16	Number of scans	16
Measurement time/ min	975	Measurement time/ min	832
Probe target temperature / K	280	Probe target temperature / K	285

Continue of **Table S3**

1D ^{1}H T1 Saturation Recovery	racemic α-TLA **2**	sulfoximine **3**
ν_r / kHz	60	60
B_0 / T	16.4	16.4
ν_1(^{1}H) / kHz	100	100
^{1}H carrier / ppm	25.3	-6.6
t_1 increments	4096	4096
Sweep width (t_1) / ppm	142.8	142.8
Acquisition time (t_1) / ms	20.5	20.5

Number of scans	8	8
Probe target temperature / K	285	285

References

1. V. Agarwal, *J. Magn. Reson.*, 2020, **311**, 106661.
2. S. A. Smith, T. O. Levante, B. H. Meier and R. R. Ernst, *J. Magn. Reson. A*, 1994, **106**, 75-105.